Alcaraz *et al.*
Sustainable Environment Research (2024) 34:22
https://doi.org/10.1186/s42834-024-00226-w

Sustainable Environment Research

RESEARCH

Open Access

Adsorption of dibenzothiophene sulfone using Fe^{3+} and Fe^{6+}-impregnated clay adsorbents

Maegan Gwyneth T. Alcaraz[1], Angelo Earvin Sy Choi[1*], Nathaniel P. Dugos[1] and Meng-Wei Wan[2*]

Abstract

In this study, the adsorption of dibenzothiophene sulfone (DBTO) was investigated using clay minerals as adsorbents. Raw bentonite (BR) and raw activated clay (ACR) were impregnated with Fe^{3+} and Fe^{6+}, creating bentonite-Fe^{3+} (BF3), bentonite-Fe^{6+} (BF6), activated clay-Fe^{3+} (ACF3), and activated clay-Fe^{6+} (ACF6). The surface functional groups, surface morphology, and surface area of the raw and modified adsorbents were studied through Fourier transform infrared spectroscopy, a scanning electron microscope, and Brunauer, Emmett, and Teller analysis, respectively. Batch experiments on simulated oil were done to test the effect of adsorption time (0.5–24 h), adsorption dosage (0.3–1.5 g), and adsorption temperature (30–50 °C). The results of the experiments showed the suitability of the pseudo-second order kinetic model on the clay adsorbent and sulfone system. This suggests that chemisorption is the rate-limiting step of the reaction. Equilibrium isotherms indicated the adherence of DBTO onto BR and BF3 to the Freundlich model, implying the heterogeneous adsorption of the sulfones onto the adsorbents. The systems of DBTO with BF6, ACR, ACF3, and ACF6 showed a better fit with the Dubinin-Radushkevich model. This denotes that adsorption happens through the filling of sulfones of the micropores on the adsorbent. Lastly, thermodynamic studies revealed the endothermic and non-spontaneous nature of the clay adsorbents and sulfone systems. The experiments showed that the impregnation of Fe^{3+} and Fe^{6+} lowered the desulfurization ability of the adsorbents. This could be due to the iron ions being hard acids and the sulfones being soft bases, thus showing lower compatibility than the raw counterparts of the adsorbents. Comparison with related studies showed that the prepared adsorbents, namely BF3 (5.1 mg g^{-1}) and BF6 (6.4 mg g^{-1}), had a higher adsorption capacity than Ni^{2+}-loaded activated carbon (4.9 mg g^{-1}) and activated clay (4.1 mg g^{-1}). The study shows that BR (7.2 mg g^{-1}) is the best-performing adsorbent, which can be set as the direction for future research. This study is a step toward the commercialization of oxidative desulfurization methods.

Keywords Desulfurization, Dibenzothiophene sulfone, Iron-impregnation, Activated clay, Bentonite, Batch adsorption

1 Introduction

The continuous improvement of technology and level of industrialization is still globally widespread. The development of businesses and connections between large and small entities results in an increase in fossil fuel consumption. The total energy demand of the Philippines in 2018 was 47 Mt of oil equivalent, wherein 89% came from fossil fuels [1]. Sulfur present in the fuel can be oxidized during combustion and form sulfur oxides. These

*Correspondence:
Angelo Earvin Sy Choi
angelo.choi@dlsu.edu.ph
Meng-Wei Wan
peterwan@mail.cnu.edu.tw
[1] Department of Chemical Engineering, De La Salle University, 0922 Manila, Philippines
[2] Department of Environmental Engineering, Chia Nan University of Pharmacy and Science, Tainan 71710, Taiwan

can turn to sulfurous and sulfuric acids, which cause corrosion in engines and exhausts. The emission of sulfur oxides into the atmosphere increases the amount of greenhouse gases, thus contributing to global warming. Additionally, sulfur dioxide and sulfate in the form of $PM_{2.5}$ in the atmosphere causes breathing difficulty, eye irritation, and cardiopulmonary diseases [2]. Thus, desulfurization processes are necessary prior to the use of fossil fuels.

Hydrodesulfurization (HDS) is the most used process for sulfur removal. Fuel is treated with hydrogen at high temperature and pressure with the use of a catalyst, which is a porous alumina matrix impregnated with combinations of Co, Ni, Mo, and W [3]. Challenges associated with the use of HDS is its costliness due to the extremely high pressure and high temperature operating conditions needed and its difficulty in removing heterocyclic sulfur compounds such as dibenzothiophene (DBT) and its derivatives [4]. These challenges pushed the development of other desulfurization processes with better cost efficiency and sulfur removal performance.

Oxidative desulfurization (ODS) utilizes oxidizing agents to remove sulfur compounds in fuel through an oxidation reaction [5]. ODS is a two-step process with the first being the oxidation of sulfur-containing compounds to create sulfoxides and sulfones, such as DBT being oxidized to dibenzothiophene sulfone (DBTO) and benzothiophene (BT) being oxidized to benzothiophene sulfone (BTO) [6]. The second process involves the removal of sulfones by liquid/liquid extraction method or adsorption [7]. A two-phase system involves the use of an aqueous oxidant to treat the fuel in the oil phase. Since the system consists of two phases, this limits the mass transfer of reactants within one another, necessitating the use of phase transfer agents, such as quaternary ammonium salts [8]. Catalysts are also used to increase the reaction rate of the oxidation process [9, 10]. With the sulfur in the fuel converted to sulfones, it can be extracted by solid adsorption, which is the focus of this study. Adsorption can selectively remove compounds with the use of solid adsorbents. Advantages of adsorption include its ability to achieve high sulfur yield at mild temperatures and pressure [11]. Additionally, adsorption can be performed at low costs using adsorbents that are regenerable and have high selectivity for sulfur compounds [12]. Commonly used adsorbents include activated carbon (AC), which is often used in purification and adsorption applications. A recent study was successful in preparing AC from polyethylene terephthalate waste for the treatment of model gasoline, reaching up to 97% DBT desulfurization at optimum conditions [13]. Another study modified AC by washing it with hydrochloric acid to improve its morphology. The increase in micro and mesoporosity resulted in about 99% DBT removal in model oil [14]. Zeolites are also commonly studied adsorbents because of their selectivity due to their highly regular structure of pores and chambers. This leads to the breaking down or exclusion of non-target molecules [15]. Because of their ability to perform cation exchange and their metal-based active site, they are commendable adsorbents for sulfur removal [16]. A study tested the ability of beta zeolite to adsorb oxidized sulfur compounds from jet and diesel fuel [17]. Results showed a decrease in sulfur from 520 and 41 to 50 and 8 ppmw, respectively. Metal organic framework (MOF)-based adsorbents are also being investigated for sulfur removal. Modification of the metal and organic linker of the MOF results in the variation of the pore size, allowing the control of adsorbent selectivity [16]. Despite the good performance of the aforementioned adsorbents, they require complex modifications and have poor thermal stability [18]. Clay minerals can be used as adsorbents with high specific areas, a variety of structural and surface properties, and chemical and mechanical stability. These adsorbents are also highly abundant and have a low cost [19]. Activated clay, bentonite, and kaolinite were tested for the adsorption of DBTO [20] and BTO [21]. The results showed that activated clay was superior to the two other adsorbents due to its surface area and the spontaneity of the process. Several studies have also tested raw bentonite for sulfur removal, wherein 67% DBT removal [22] and 73% BTO removal [21] were obtained. Studies have investigated the impregnation of clay adsorbents with Cu [23], Na [24], and Zn [25] to improve its desulfurization performance by modifying the interaction of the metal with the sulfur. To date, no information was available on the use of Fe-impregnated clay adsorbents to remove DBTO from simulated oil.

This study investigated the ability of Fe^{3+} and Fe^{6+}-impregnated bentonite and activated clay to remove DBTO from simulated oil through batch experiments. The raw and modified adsorbents underwent Fourier transform infrared spectroscopy (FTIR) to determine the functional groups essential for sulfone adsorption. The adsorbents were also investigated under a scanning electron microscope (SEM) to observe their surface morphology. Brunauer, Emmett, and Teller (BET) surface area analysis was done to quantify the specific surface area of the adsorbents. The effect of adsorption time, adsorbent dosage, and adsorption temperature on sulfone removal was tested. The adsorption time and temperature were studied to gain an idea of the time to reach equilibrium and temperature for maximum sulfone removal. It is imperative to arrive at the optimal operating time and temperature since the control of these parameters is correlated to the operating costs of desulfurization units.

Adsorbent dosage must also be studied to maximize the use of resources for sulfur removal. Kinetic, isotherm, and thermodynamic analysis were also performed to gain insight into the mechanism of DBTO onto the clay adsorbents. The effect of Fe-impregnation on sulfone removal was investigated and compared with existing studies.

2 Experimental

2.1 Materials

Bentonite was obtained from Seimao Chemical Material Co. Activated clay was procured from Alfa Aesar. Ferric nitrate nonahydrate ($Fe(NO_3)_3{\cdot}9(H_2O)$, 100%), potassium hydroxide pellets (KOH, 100%), and toluene (C_7H_8, 99.8%) was purchased from Sigma-Aldrich. Potassium ferrate (K_2FeO_4, 95 wt%) was acquired from Lab Tools. DBTO ($C_{12}H_8O_2S$, 98 wt%) was obtained from Tokyo Chemical Industry.

2.2 Instrumental analysis

FTIR was performed on the raw and modified adsorbents to determine the functional groups present on the surface of the adsorbents. The adsorbents were crushed and homogenized with KBr using a mortar and pestle in a 1:20 ratio, then pelletized and examined at frequencies of 400 to 4000 cm^{-1} with the JASCO FTIR 410. The specific surface area of the adsorbents before adsorption was analyzed using the BET multipoint technique using the N_2 isotherm at 77 K. The morphology of the raw and modified adsorbents was investigated under a SEM. A Hitachi S-3000N SEM was used, operated under a tungsten filament for its vacuum and 20 kV of accelerating voltage. A sputter coater was utilized to create a thin layer of gold on the surface of the samples. The concentration of DBTO in the simulated oil was determined using an Agilent 7890A gas chromatograph (GC) with an Agilent 355 sulfur chemiluminescence detector (SCD). The initial temperature of the GC oven was set to 200 °C for 1 min and raised by 20 °C every min until it reached 280 °C, which was retained for 1 min.

2.3 Metal impregnation

The procedure for impregnation was patterned on the study of Chen et al. [26]. For the impregnation of Fe^{3+}, a 0.1 M $Fe(NO_3)_3$ solution was prepared. Bentonite and activated clay were mixed with the solution in a 1 g: 10 mL ratio. For the impregnation of Fe^{6+}, 0.025 M K_2FeO_4 was prepared with deionized water. An adsorbent-to-solution ratio of 1 g: 10 mL was used for the mixing of bentonite and activated clay with Fe^{6+} solution. KOH was used to maintain an alkaline environment (around pH 10) to keep ferrate stable. The adsorbents in the solution with their corresponding iron salt were constantly stirred with a magnetic stirrer for 12 h. The suspensions were filtered and the adsorbents were transferred to a petri dish to be left to dry in an oven for 12 h at 120 °C. The dried adsorbents were then crushed and ground with a mortar and pestle and passed through a 100-mesh (150 μm) sieve. The underflow was then stored for future use. Adsorbents used were raw bentonite (BR), bentonite-Fe^{3+} (BF3), bentonite-Fe^{6+} (BF6), raw activated clay (ACR), activated clay-Fe^{3+} (ACF3), and activated clay-Fe^{6+} (ACF6).

2.4 Batch experimental studies

A 500 ppm S solution was prepared by dissolving 3.44 g DBTO in toluene. The effect of adsorption time was observed by mixing 30 mL of the simulated fuel with 1 g of the adsorbent and stirring using a temperature-controlled water bath shaker at 110 rpm and room temperature. Samples were collected from 0.5 to 24 h. The same range of adsorption time was used in a similar study investigating the removal of sulfones from synthetic fuel [27].

The effect of adsorbent dosage was investigated by using 30 mL of the simulated fuel and varying the dosage from 0.3 to 1.5 g. This is similar to the range of parameters used by a related study, wherein they used 0.25 to 1.5 g adsorbent to desulfurize model oil [22]. The mixture was mixed at 110 rpm and room temperature for 24 h.

The effect of temperature was analyzed by placing 1 g of the adsorbent in 30 mL of the simulated fuel. Similar to a previous study, the tested adsorption temperatures were 30, 40, and 50 °C [21]. The system was mixed at 110 rpm until equilibrium.

The DBTO concentration of the samples was determined using GC-SCD and the sulfone removal and adsorption capacity were calculated using Eqs. (1) and (2), respectively.

$$C_e = \frac{C_o - C_e}{C_o} \times 100 \tag{1}$$

$$q_e = \frac{C_0 - C_e}{m} xV \tag{2}$$

where q_e stands for the adsorption capacity at equilibrium (mg g^{-1}), C_o is the initial concentration (mg L^{-1}), C_e is the equilibrium concentration (mg L^{-1}), m is the mass of the adsorbent (g), and V is the volume of solution (L).

3 Results and discussion

3.1 FTIR analysis

The functional groups found on the surface of the adsorbent have a large effect on its adsorption performance. A graph of the FTIR spectra of the raw and modified adsorbents is shown in Fig. 1. The peaks of

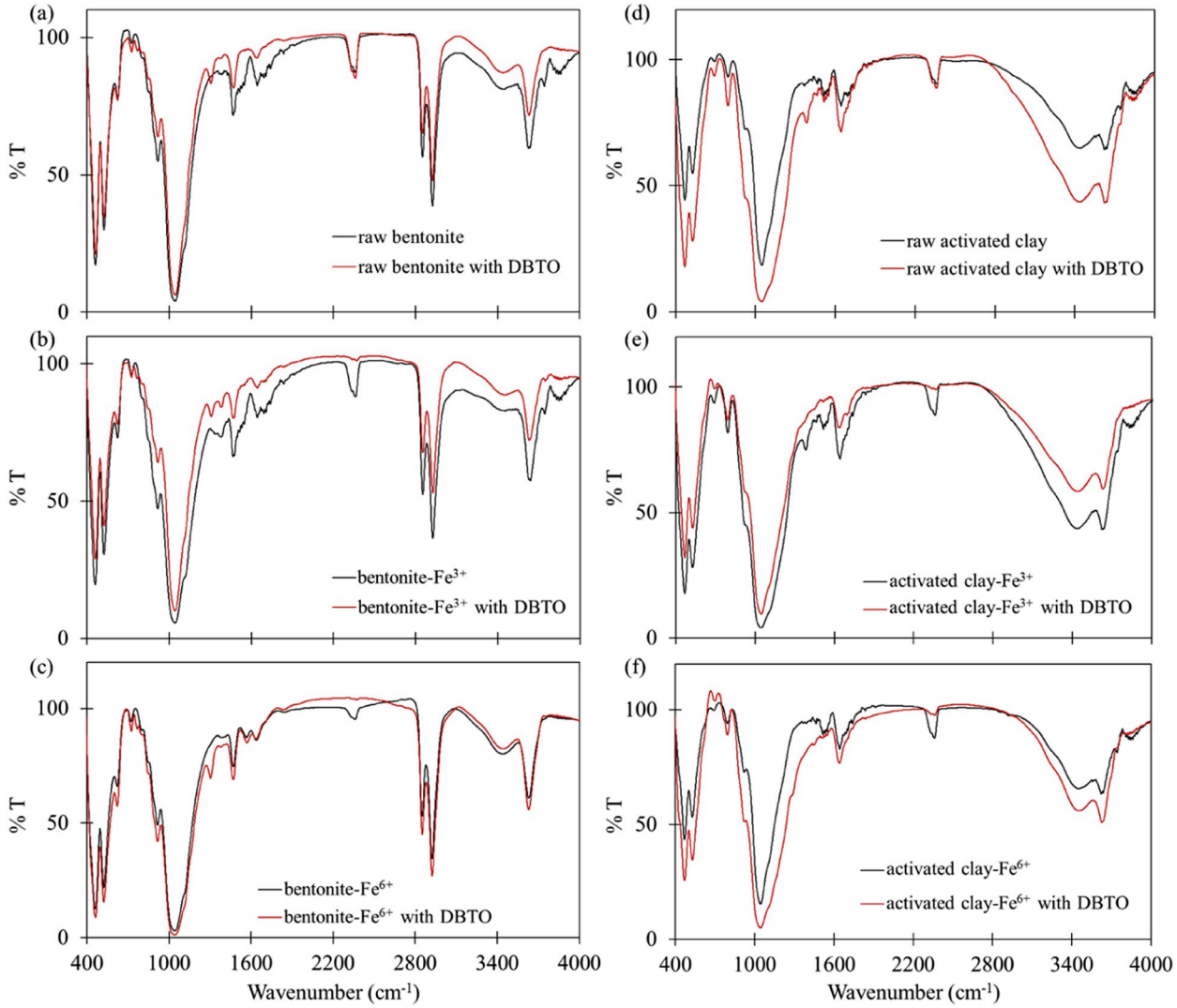

Fig. 1 FTIR spectra of (**a**) raw bentonite, (**b**) bentonite-Fe^{3+}, (**c**) bentonite- Fe^{6+}, (**d**) raw activated clay, (**e**) activated clay-Fe^{3+}, and (**f**) activated clay-Fe^{6+} before and after DBTO adsorption

BF3 and BF6 show close similarity with the peaks of BR. The same can be said with the peaks of ACF3 and ACF6 showing the same shape as ACR. From there, it can be deduced that the same functional groups present in the raw adsorbents can be found in the impregnated adsorbents. The iron ions impregnated on the adsorbent cannot be detected in the FTIR analysis and can be considered IR inactive. This is because to be IR active, the molecule must absorb IR. This happens when there is a change in the dipole moment of the functional group and the resulting frequency of the vibration matches that of the frequency of the radiation [28]. Since an iron ion does not have a dipole moment, it cannot absorb IR and will not be detected in an FTIR analysis.

The FTIR spectra of the different bentonite and activated clay adsorbents before and after the adsorption of DBTO are shown in Fig. 1. The strong peak at 1044 cm^{-1} corresponds to C-O stretching [29]. The peak at 1638 cm^{-1} can be attributed to the N–H bending in the amide group [20]. C-H stretching corresponds to the peaks at 2851 and 2924 cm^{-1} [30]. The broad band at 3437 cm^{-1} is attributed to the O–H stretching from hydroxyl, carboxylic, and phenolic functional groups [31]. O–H stretching from free alcohols also results in a band at 3625 cm^{-1}.

The shifts in peaks of the adsorbents before and after sulfone adsorption indicate the involvement of the corresponding functional group. BR and BF3 had a notable shift in peak from 3629 to 3625 cm^{-1} and 3628 to

3627 cm^{-1}, respectively, after DBTO adsorption. This implies that the stretching of hydroxyl groups (-OH) aided in DBTO adsorption. The adsorption of DBTO onto raw ACR can also be related to the presence of hydroxyl groups as the adsorbent wavelength shifted from 3621 to 3628 cm^{-1} after adsorption. The shift in wavelength from 1643 to 1638 cm^{-1} with the use of ACF3 can be attributed to the involvement of amine (-NH) groups. Lastly, the adsorption of DBTO onto ACF6 showed a peak shift from 3621 to 3628 cm^{-1}, attributed to the stretching of hydroxyl groups on the adsorbent. A mechanism is proposed regarding the involvement of hydroxyl groups in most of the adsorbents. The polar character of DBTO increases due to the presence of the double-bonded oxygens. Since the hydroxyl group on the adsorbent also exhibits a polar character, a bond is formed between them. Specifically, the lone pairs of the oxygen on the sulfone react with the oxygen on the hydroxyl group and form a covalent bond. This bond allows the sulfone to be adsorbed from the solution.

3.2 SEM analysis

The raw and modified adsorbents were analyzed under SEM to investigate the effect of metal impregnation on the surface morphology of the adsorbents. The SEM images of the raw and impregnated bentonite and activated clay are shown in Fig. 2. The surface of BR consists of non-uniform particles with smooth layers. The

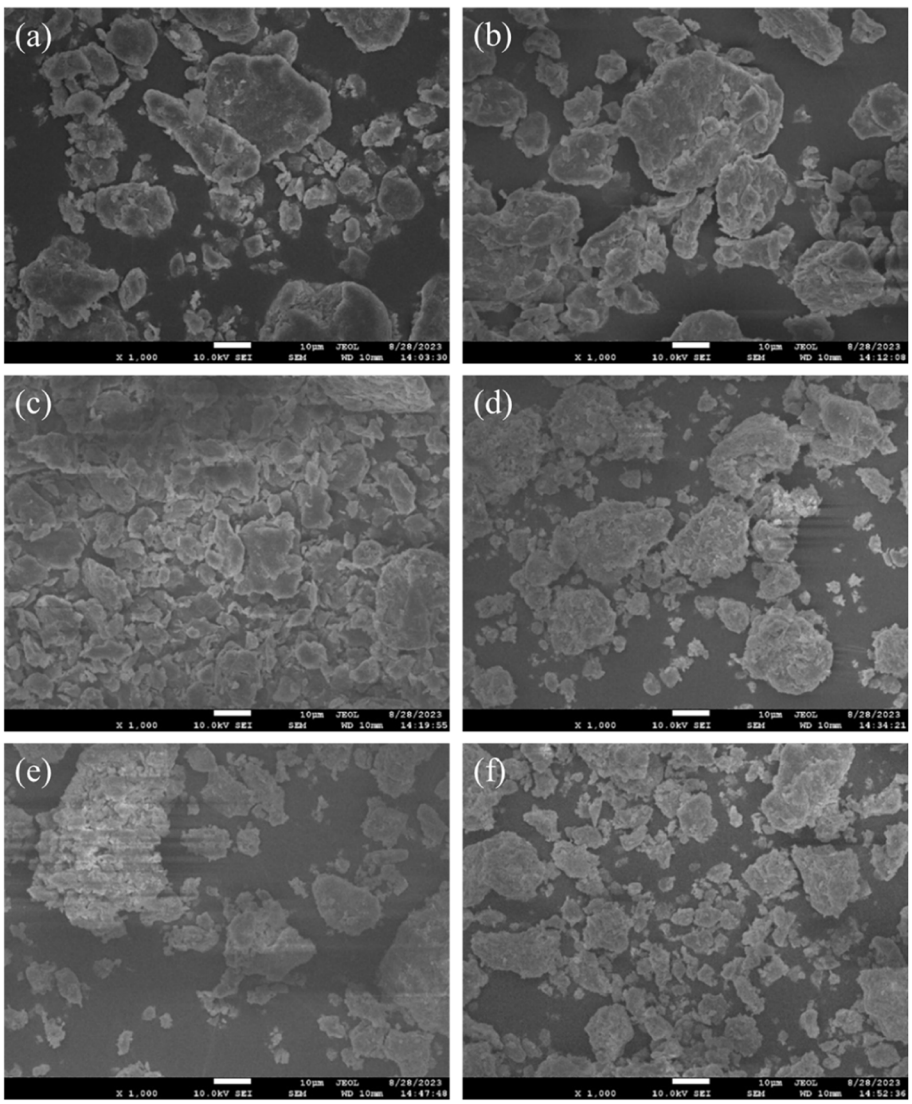

Fig. 2 SEM micrographs of (**a**) raw bentonite, (**b**) bentonite-Fe^{3+}, (**c**) bentonite- Fe^{6+}, (**d**) raw activated clay, (**e**) activated clay-Fe^{3+}, and (**f**) activated clay-Fe^{6+}

surface of ACR also shows non-uniform particles with a more ragged surface. A porous surface is more conducive to adsorption as this reduces the resistance faced by the adsorbed molecules [32]. This also facilitates the diffusion of the adsorbate from the solution to the surface of the adsorbate. After impregnation of the raw adsorbents with Fe^{3+}, the particles appear to have conglomerated, resulting in a larger particle size. This is less conducive to adsorption as the clumping of particles results in less accessible active sites on the surface. After the impregnation of bentonite with Fe^{6+}, a large reduction in surface area can be observed with more deposits on the surface of the adsorbent. Fe^{6+} impregnation on activated clay also displayed the depositing of particles on the surface, accompanied by the reduction of particle size of the adsorbent.

3.3 BET analysis

The raw and modified adsorbents were analyzed through BET to determine their specific surface area and these are listed in Table 1. It can be seen that activated clay has the highest surface area compared to all the other adsorbents. This is because of the activation process, which is done to improve the performance of several adsorbents.

Table 1 BET surface area of fresh adsorbents

Adsorbent	BET Surface Area (m^2 g^{-1})
Raw bentonite	6.6
Bentonite-Fe^{3+}	4.9
Bentonite-Fe^{6+}	2.7
Raw activated clay	93
Activated clay-Fe^{3+}	88
Activated clay-Fe^{6+}	58

Through physical or chemical methods, activation is performed to increase the degree of pore development and subsequently, the surface area of adsorbents [33]. From the data, it is observed that the surface area of the raw and modified adsorbents is arranged in the following order: raw > Fe^{3+} > Fe^{6+}. The treatment with the metals decreased the surface area of the adsorbents. This coincides with the SEM images, wherein impregnation with iron resulted in the clumping of the adsorbents. It is also hypothesized that the iron molecules blocked the pores of the adsorbent, which resulted in a lower specific surface area.

3.4 Kinetic studies

A study on the effect of the adsorption time of the sulfone and adsorbent system is necessary for the determination of the equilibrium time and to improve the design of future processes. The desulfurization of bentonite and activated clay adsorbents for DBTO removal at different adsorption times are shown in Fig. 3. A fast rise in desulfurization was observed during the first hour, indicating that the adsorption sites were rapidly filled during this period. After this time, a slow increase in desulfurization with the progress of adsorption time can be due to the gradual access of unoccupied adsorption sites [11].

The data showed that raw adsorbents were able to remove a higher amount of sulfur as compared to the impregnated adsorbents. The lowering of desulfurization performance using the impregnated adsorbent can be attributed to the Hard and Soft Acids and Bases (HSAB) principle. The HSAB principle implies that soft acids prefer binding with soft bases, and hard acids prefer binding with hard bases [34]. Fe^{3+} and Fe^{6+} have empty orbitals due to their oxidation state, making them electron pair acceptors. The lack of electrons also denotes the strong effect of the nucleus on the electron cloud, making it difficult

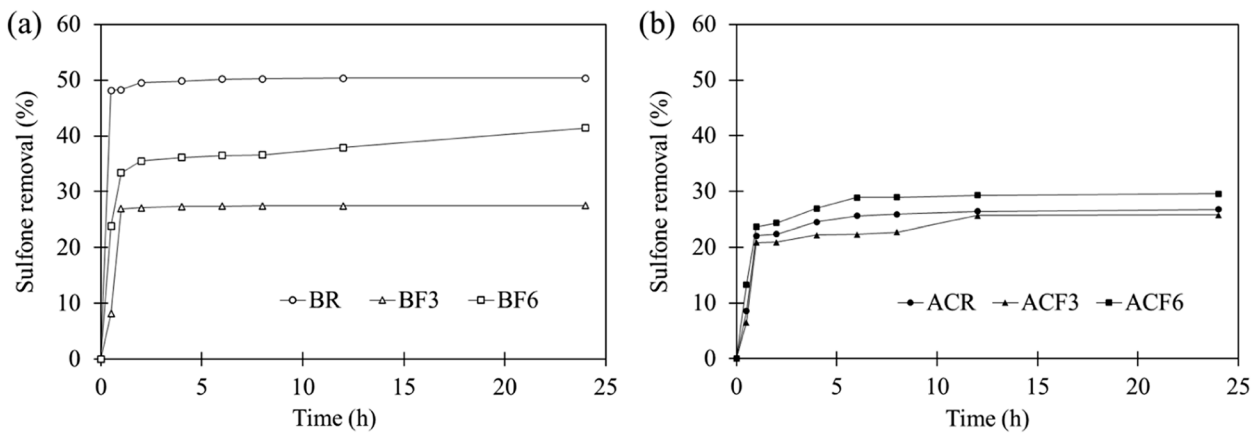

Fig. 3 Sulfone removal of DBTO at different adsorption times onto **a** bentonite adsorbents and **b** activated clay adsorbents

to polarize. Because of this, Fe^{3+} and Fe^{6+} are considered hard acids. On the other hand, sulfones are considered soft bases because of the lone pairs of electrons on oxygen and their high polarizability. The presence of benzene rings in DBTO indicates the delocalization of electrons. This results in the electrons being easier to move around the molecule, making the sulfones highly polarizable, and in turn, soft bases. The impregnation of iron on bentonite and activated clay resulted in a lower affinity for sulfones and weakened the interaction between the sulfone and adsorbents. From Sect. 3.2, the morphology of the adsorbents showed a decrease in surface area after impregnation, which is in accordance with the specific surface area data collected in Sect. 3.3. Since the specific surface area decreased after impregnation, this implies that the metal was deposited on the adsorbent. However, the impregnation with iron might have covered the polar molecules already present in the adsorbent. Aiming to increase the polarity by metal impregnation could have affected the polar molecules already available on the adsorbents, thus lowering the desulfurization. Additionally, Fe^{6+}-impregnated adsorbents showed higher sulfur removal than Fe^{3+}-impregnated adsorbents. Since the number of valence electrons of Fe^{6+} is less than that of Fe^{3+}, it results in Fe^{6+} being smaller in size and subsequently, more reactive than Fe^{3+}. This results in a higher affinity of the sulfur with the adsorbents impregnated with Fe^{6+}.

The pseudo first-order equation, shown in Eq. (3), indicates a reversible system between the adsorbent and adsorbate [35]. The adherence of a system to the pseudo second-order rate equation, listed in Eq. (4), indicates that chemisorption limits the rate of the reaction. This involves valence forces by the sharing or exchanging of electrons between the adsorbate and adsorbent [36].

$$ln(q_t - q_e) = lnq_t - k_1 t \tag{3}$$

$$\frac{t}{q_e} = \frac{1}{k_2 q_t^2} + \frac{1}{q_t} t \tag{4}$$

where q_t is the adsorption capacity at a given time (mg g^{-1}), k_1 is the pseudo first-order adsorption rate constant (min^{-1}), k_2 is the pseudo second-order adsorption rate constant (g mg^{-1} min^{-1}), and t is the reaction time (min).

The kinetic parameters and coefficients of determination (R^2) of the different kinetic model equations on BR, BF3, BF6, ACR, ACF3, and ACF6 for DBTO removal are shown in Table 2. The results indicate adherence to the pseudo-second order model with a high R^2 value and similar values for the experimental and theoretical q_e. This implies that chemisorption is the rate-limiting step of the reaction between the clay adsorbents and the sulfur compounds. This also supports the proposed mechanism wherein covalent bonds form between the sulfone and the responsible functional groups on the surface of bentonite, allowing the sharing of electrons [20]. The calculation of the pseudo-second order rate constant, k_2, can provide insights into the speed of the reaction. A large value of k_2 implies a relatively faster reaction, while a small value implies a slower reaction. From the calculation of k_2, BR had the highest value, which is almost 16 times as fast as the slowest reaction, which is BF6. These experimental rate constant values can be used for application to reactor design and upscaling efforts.

A comparison of the experimental data with the calculated data from kinetic models of DBTO adsorption onto BR is shown in Fig. 4. The theoretical values calculated from the pseudo-first order model largely deviate from the experimental data. The modelled data from the pseudo-second order model closely follow the experimental data, implying a better fit of the pseudo-second order model to the system compared to the pseudo-first order model. This coincides with the high values of R^2 found in Table 2 for the pseudo-second order model.

3.5 Isotherm studies

Studying the effect on adsorption with varying adsorbent dosages is vital to be able to reach maximum sulfur removal at an economic amount of adsorbent. The DBTO removal of clay adsorbents at different adsorbent

Table 2 Kinetic parameters for DBTO adsorption on BR, BF3, BF6, ACR, ACF3, and ACF6

Model	Parameter	BR	BF3	BF6	ACR	ACF3	ACF6
	$q_{e,exp}$ (mg g^{-1})	7.55	4.12	6.21	4.01	3.87	4.43
PseudoFirst Order	k_1 (min^{-1})	8.2×10^{-3}	9.4×10^{-3}	2.4×10^{-3}	5.5×10^{-3}	6.0×10^{-3}	6.2×10^{-3}
	$q_{e,theo}$ (mg g^{-1})	0.82	0.67	2.2	1.8	2.6	2.0
	R^2	0.8112	0.7568	0.5645	0.8740	0.8125	0.8966
PseudoSecond Order	k_2 (g mg^{-1} min^{-1})	6.2×10^{-2}	1.3×10^{-2}	3.9×10^{-3}	7.6×10^{-3}	4.6×10^{-3}	8.9×10^{-3}
	$q_{e,theo}$ (mg g^{-1})	7.6	4.2	6.3	4.1	4.0	4.5
	R^2	0.9999	0.9975	0.9972	0.9989	0.9966	0.9997

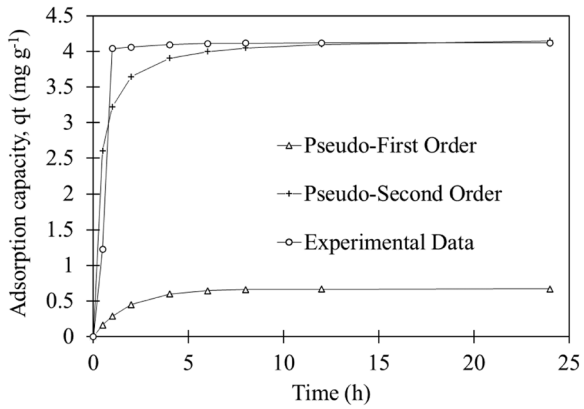

Fig. 4 Comparison of experimental data with modelled data from different kinetic models on DBTO adsorption using BR

dosages is shown in Fig. 5. Increasing the adsorbent amount increases the active sites available for adsorption, and subsequently, the sites where the sulfur molecules can adhere [37].

The Langmuir model assumes that the adsorbed layer has a thickness of only one molecule and that there should be no steric hindrance and interaction between adjacent adsorbed molecules [38]. Also, it assumes that once a molecule has occupied an adsorption site, no further adsorption will occur at that site. The linearized form of the Langmuir model is shown in Eq. (5).

$$\frac{1}{q_e} = \frac{1}{K_L q_m}\frac{1}{C_e} + \frac{1}{q_m} \tag{5}$$

where q_m is the adsorption capacity when monolayer coverage is achieved (mg g^{-1}), and K_L is the Langmuir adsorption constant (L mg^{-1}).

The Freundlich model does not restrict multilayer adsorption, in contrast with the Langmuir isotherm. It assumes that the compound is adsorbed at various sites of heterogeneous adsorbent with varying adsorption heat and affinities [15]. The stronger binding sites will first be occupied by the adsorbate. The adsorption energy will then exponentially decline as the adsorption reaches equilibrium [38]. The equation for the Freundlich model is shown in Eq. (6).

$$logq_e = logK_F + \frac{1}{n}logC_e \tag{6}$$

where K_F is the Freundlich constant (mg g^{-1}), and n is an indication of the adsorption capacity. If 1/n is greater than zero and less than one ($0 < 1/n < 1$), the adsorption process is favorable; while if 1/n is greater than one, the adsorption process is unfavorable. A value of 1 for 1/n signifies an irreversible process.

The Dubinin-Radushkevich (DR) model was formed to account for the effect of the porosity of an adsorbent [39]. It assumes that adsorption progresses through pore-filling and that physical multilayer adsorption is possible through Van der Waals forces [40]. The linearized equation for the model is shown in Eq. (7).

$$lnq_e = q_s - K_D\varepsilon^2 \tag{7}$$

where q_s is the theoretical saturation capacity (mg g^{-1}), and K_D is the DR isotherm constant (mol^2 kJ^{-2}). The variable ε is the adsorption potential, which can be calculated using Eq. (8).

$$\varepsilon = RTln(1 + \frac{1}{C_e}) \tag{8}$$

where R is the universal gas constant taken as 8.314 J mol^{-1} K^{-1}, and T is the absolute temperature (K).

The Temkin model considers the interaction of the adsorbent and adsorbate. This model assumes, excluding

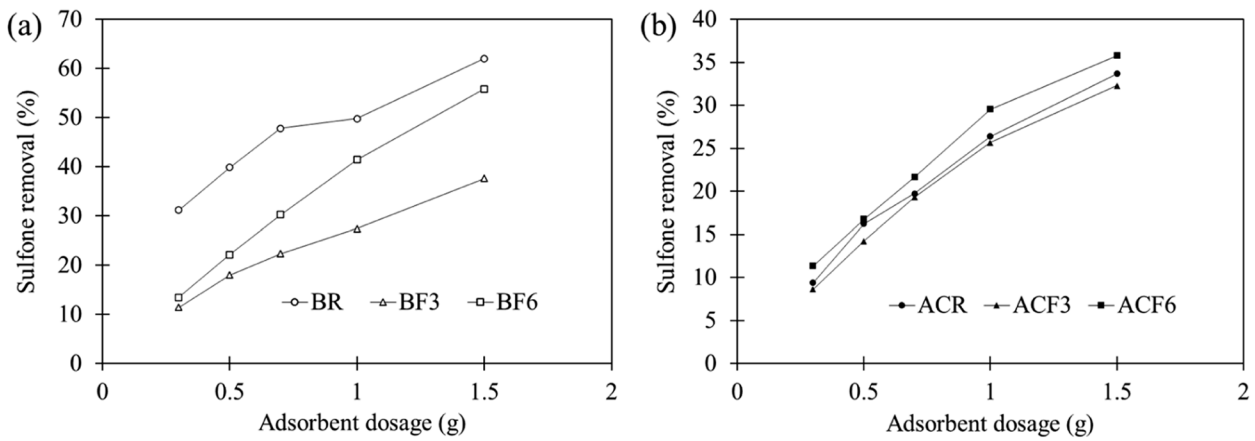

Fig. 5 Sulfone removal of DBTO at different adsorbent dosages onto (**a**) bentonite adsorbents and (**b**) activated clay adsorbents

very low and very large concentration values, that the adsorption heat of the molecules present on the surface of the adsorbent declines linearly with adsorbate coverage on the adsorbent [38]. The equation for this model is shown in Eq. (9).

$$q_e = \frac{RT}{B_T} lnA_T + \frac{RT}{B_T} \ln C_e \quad (9)$$

where A_T is the Temkin isotherm equilibrium binding constant (L mg^{-1}), and B_T is the Temkin constant related to the heat of adsorption (J mol^{-1}) [41].

The calculated adsorption parameters and coefficients of determination (R^2) of the different isotherm model equations on BR, BF3, BF6, ACR, ACF3, and ACF6 for DBTO removal are shown in Table 3. It is observed that the best-fit model for BR and BF3 is the Freundlich model, which denotes that the adsorption of sulfones onto the adsorbents occurs on a multilayer mechanism. This also implies that the stronger binding sites are occupied first. Additionally, since the value of 1/n for BR and BF3 are greater than one, it can signify that the process is unfavorable and that other modifications can benefit the system. The other adsorbents, specifically BF6, ACR, ACF3, and ACF6, adhere to the DR isotherm. This model accounts for the effect of the porosity of the adsorbent and assumes that adsorption happens through pore filling instead of film formation on the walls of pores. The value of q_s in the DR isotherm gives the theoretical saturation capacity of the adsorbent. This indicates the maximum adsorption capacity that an adsorbent can achieve if conditions are closest to an ideal system. The values for q_s of the adsorbents are approximately 1.5 times that of the experimental equilibrium adsorption capacity. This is expected for calculated theoretical values as these do not account for resistances and interactions.

A comparison of the calculated data from isotherm models and the experimental data from DBTO adsorption onto BF6 is presented in Fig. 6. Close values between the experimental and calculated data are observed with minimal differences across the four isotherms. Values from the DR isotherm show the closest similarity with the experimental data. This is in accordance with BF6 having the highest R^2 in the testing of the different isotherm models to the sulfone and clay adsorbent system.

3.6 Thermodynamic studies

Temperature is a necessary parameter to define for unit processes since this affects the reaction rate of the process and the quality of the reactants. The desulfurization performance of BR, BF3, BF6, ACR, ACF3, and ACF6 for DBTO removal at different reaction temperatures is shown in Fig. 7. Raising the temperature increases desulfurization due to the increase in the kinetic energy of the particles in the system [42]. This gives higher chances

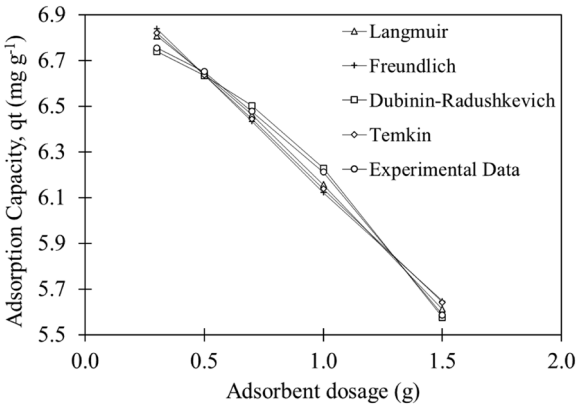

Fig. 6 Comparison of experimental data with modelled data from different isotherm models on DBTO adsorption using BF6

Table 3 Isotherm parameters for DBTO adsorption on BR, BF3, BF6, ACR, ACF3, and ACF6

Model	Parameter	BR	BF3	BF6	ACR	ACF3	ACF6
Langmuir	K_L (L mg^{-1})	3.63×10^{-5}	6.75×10^{-6}	8.10×10^{-3}	7.25×10^{-2}	3.29×10^{-2}	8.45×10^{-2}
	q_m (mg g^{-1})	659	1441	9	1686	3461	1365
	R^2	0.9077	0.9320	0.9933	0.9125	0.8881	0.9370
Freundlich	K_F (mg g^{-1})	1.48×10^{-3}	2.20×10^{-3}	1.21	4.28×10^{-3}	1.29×10^{-2}	2.29×10^{-3}
	n	0.63	0.78	3.51	0.87	1.05	0.78
	R^2	0.9135	0.9344	0.9771	0.8901	0.8804	0.9422
Dubinin-Radushkevich	K_D (mol^2 kJ^{-2})	7.39×10^{-3}	1.38×10^{-2}	2.04×10^{-3}	1.40×10^{-2}	1.22×10^{-2}	1.46×10^{-2}
	q_s (mg g^{-1})	19.71	8.56	7.21	7.42	6.39	8.65
	R^2	0.8249	0.8943	0.9983	0.9175	0.9310	0.9441
Temkin	A_T (L mg^{-1})	7.30×10^{-3}	5.82×10^{-3}	1.13×10^{-1}	6.29×10^{-3}	7.53×10^{-3}	5.85×10^{-3}
	B_T (J mol^{-1})	158	414	588	530	685	427
	R^2	0.8792	0.9213	0.8768	0.8805	0.9004	0.9436

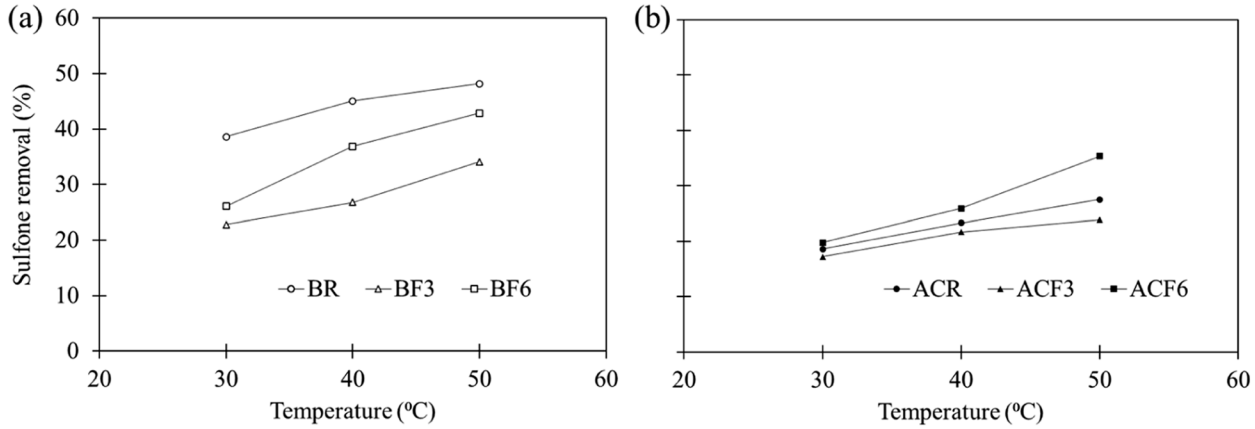

Fig. 7 Sulfone removal of DBTO at different temperatures onto **a** bentonite adsorbents and **b** activated clay adsorbents

of effective collisions between the adsorbents and sulfur particles, and therefore, a push in the progress of the adsorption process.

To further characterize the adsorption system, thermodynamic parameters such as enthalpy (ΔH), entropy (ΔS), and Gibbs free energy (ΔG) can be calculated. The adsorption coefficient (K_d), which is given by Eq. (9), is defined by the ratio of the adsorbate adsorbed and the adsorbate concentration remaining in the solution.

$$K_d = \frac{q_e}{C_e} \tag{10}$$

where q_e is the adsorption capacity at equilibrium, also considered as the amount of adsorbate on the adsorbent (mg g^{-1}).

Equation (11) is used to solve for ΔG at different temperatures [20]. The definition of ΔG is given in Eq. (12). By substituting this into Eq. (11), the expression in Eq. (13) can be used to identify ΔS and ΔH from the variation of system temperature [43].

$$\Delta G = -RTlnK_d \tag{11}$$

$$\Delta G = \Delta H - T\Delta S \tag{12}$$

$$lnK_d = \frac{\Delta S}{R} - \frac{\Delta H}{R}\frac{1}{T} \tag{13}$$

An analysis of the thermodynamic properties of the clay adsorbents and sulfone systems was performed and the parameters are listed in Table 4. Positive values for ΔG at all temperatures indicate the non-spontaneity of the adsorption process with the adsorbents at 30 to 50 °C. The decreasing value of ΔG with increasing temperature also indicates the favorability of the adsorption process at higher temperatures [20]. It can also be observed that BR has the lowest ΔG at all temperatures among the tested adsorbents. This agrees with BR having the highest desulfurization across the other adsorbents since the lower ΔG indicates higher spontaneity and proceeding of the adsorption reaction. With the ΔH values being positive for all the adsorbents, this implies that the process of sulfone adsorption onto the clay adsorbents is endothermic. This is in accordance with the findings of the study that sulfone desulfurization increases with the increase in temperature. Positive values for ΔS denote the increase in entropy or randomness during the adsorption process. Physical implications of a positive ΔS value include increased randomness at the interface of the liquid and adsorbent [44]. This suggests structural changes in the adsorbent and adsorbate, wherein the sulfur being removed becomes attached to the surface of the adsorbent.

3.7 Comparison with related research

The raw and modified adsorbents used in this study were compared with other research that investigated the removal of DBTO from simulated oil in Table 5. It can be seen that activated carbon loaded with Ni^{2+} from the study of Chen et al. [26] achieved the highest sulfur removal at 99%. 61% removal was achieved with activated clay in the study of Choi et al. [20], while the present study reached only 48% sulfur removal with bentonite. Despite this, the adsorption capacity of the adsorbents used in the present study was revealed to be higher than that of previous works. The modified Fe^{3+} and Fe^{6+}-impregnated bentonite had a higher adsorption capacity than the other presented adsorbents despite having poorer performance than raw bentonite. BR reached 7.2 mg g^{-1} which is the highest capacity among the listed adsorbents. Clay adsorbents are cheap and stable and the performed method for Fe impregnation is considerably

Table 4 Thermodynamic parameters for DBTO adsorption on BR, BF3, BF6, ACR, ACF3, and ACF6

Adsorbent	Temperature (°C)	ΔG (kJ mol^{-1})	ΔH (kJ mol^{-1})	ΔS (kJ mol^{-1} K^{-1})
BR	30	10.0	16	0.020
	40	9.6		
	50	9.6		
BF3	30	11.9	23	0.036
	40	11.7		
	50	11.2		
BF6	30	11.5	31	0.064
	40	10.5		
	50	10.2		
ACR	30	12.6	21	0.027
	40	12.2		
	50	12.0		
ACF3	30	12.8	17	0.013
	40	12.5		
	50	12.5		
ACF6	30	12.4	32	0.066
	40	11.9		
	50	11.0		

Table 5 Comparison of findings of related research on DBTO adsorption

Adsorbent	Modification	Sulfur removal (%)	Adsorption capacity (mg g^{-1})	Reference
Activated carbon	-	70	3.5	[26]
	Cu^{2+}-loaded	98	4.9	
	Fe^{3+}-loaded	98	4.9	
	Ni^{2+}-loaded	99	4.9	
Activated clay	-	61	3.1	[20]
Bentonite	-	47	2.4	
Kaolinite	-	30	1.5	
Bentonite	-	48	7.2	Present study
	Fe^{3+}-loaded	34	5.1	Present study
	Fe^{6+}-loaded	43	6.4	Present study
Activated clay	-	28	4.1	Present study
	Fe^{3+}-loaded	24	3.6	Present study
	Fe^{6+}-loaded	35	5.3	Present study

simple. Further study can be done to capitalize on the adsorption capabilities of clay adsorbents.

4 Conclusions

Clay adsorbents, specifically, bentonite and activated clay, were impregnated with Fe^{3+} and Fe^{6+} to test their effect on the removal of DBTO from simulated oil. Hydroxyl groups were found to be the main functional group for BR, BF3, BF6, ACR, and ACF6, while amine groups were essential for DBTO adsorption onto ACF3. SEM imaging and BET analysis showed that the impregnation of Fe resulted in the conglomeration of adsorbent particles and deposition of particles on the surface, thus reducing the surface area of the adsorbent. Kinetic studies showed the adherence of the clay adsorbent and sulfone systems to the pseudo-second order model, implying that chemisorption is the rate-limiting step of the reaction. Equilibrium isotherm studies showed that the systems of DBTO with BR and BF3 adhered to the Freundlich model. This implies that the adsorption of the adsorbate onto the adsorbent happens through a heterogeneous and multilayer mechanism. On the other hand, the systems of DBTO with BF6, ACR, ACF3, and ACF6 showed adherence to the DR model. This model accounts for the porosity of the adsorbent and assumes that the adsorbate fills the micropores of the adsorbent. Thermodynamic studies showed the endothermic and non-spontaneous nature of the clay adsorbent and sulfone systems. These results signify the viability of using raw and impregnated clay adsorbents for the removal of sulfone from oil. A study of the effect of different parameters showed that an increase in dosage could further increase the sulfone removal of the adsorbents. The endothermic nature of the system also implies that higher temperatures should be tested to observe higher desulfurization rates. This study also suggests that future research can focus on the enhancement of the chemical properties of the adsorbent as chemisorption plays a large part in the adsorption process. It was revealed that Fe-impregnated adsorbents

had a higher adsorption capacity than related research. However, raw bentonite still performed the best out of all the tested adsorbents and can be further investigated to arrive at a suitable adsorbent for sulfone removal.

Acknowledgements
The authors would like to acknowledge the Department of Science and Technology of the Philippines through its Engineering Research and Development for Technology program and the Ministry of Science and Technology for providing financial support.

Authors' contributions
Maegan Alcaraz performed the experiments and wrote the manuscript. Angelo Choi, Nathaniel Dugos, and Meng-Wei Wan provided guidance and consultation and refined the manuscript. All authors reviewed the final manuscript.

Funding
This work was supported by the Ministry of Science and Technology (MOST 111–2221-E-041–002-MY3).

Availability of data and materials
The datasets collected and analyzed for the current study are available from the corresponding author upon reasonable request.

Declarations

Competing interests
The authors declare they have no competing interests.

Received: 26 December 2023 Accepted: 12 August 2024
Published online: 03 September 2024

References

1. Vergel KBN, Marcelo KRS, Salison AJP, Elamparo FNM, Saavedra VAL, Villedo KP, et al. Estimation of transportation energy demand of the Philippines using a bottom-up approach. Asian Transp Stud. 2022;8:100058.
2. Khaniabadi YO, Polosa R, Chuturkova RZ, Daryanoosh M, Goudarzi G, Borgini A, et al. Human health risk assessment due to ambient PM_{10} and SO_2 by an air quality modeling technique. Process Saf Environ. 2017;111:346–54.
3. Fahim MA, Alsahhaf TA, Elkilani A. Hydroconversion. In: Fahim MA, Alsahhaf TA, Elkilani A, editors. Fundamentals of Petroleum Refining. Amsterdam: Elsevier; 2010. p. 153–98.
4. Srivastava VC. An evaluation of desulfurization technologies for sulfur removal from liquid fuels. RSC Adv. 2012;2:759–83.
5. Rajendran A, Cui TY, Fan HX, Yang ZF, Feng J, Li WY. A comprehensive review on oxidative desulfurization catalysts targeting clean energy and environment. J Mater Chem A. 2020;8:2246–85.
6. Haboc MM, Dugos NP, Choi AES, Wan MW. A review on the current and potential oxidant-catalyst systems in mixing-assisted oxidative desulfurization. Chem Engineer Trans. 2023;103:559–64.
7. Hossain MN, Park HC, Choi HS. A comprehensive review on catalytic oxidative desulfurization of liquid fuel oil. Catalysts. 2019;9:229.
8. Flores R, Rodas A, Gasperin R. Oxidative desulfurization of diesel fuel oil using supported Fenton catalysts and assisted with ultrasonic energy. Petrol Sci. 2019;16:1176–84.
9. He L, Li H, Zhu W, Guo J, Jiang X, Lu J, et al. Deep oxidative desulfurization of fuels using peroxophosphomolybdate catalysts in ionic liquids. Ind Eng Chem Res. 2008;47:6890–5.
10. Wang H, Jibrin I, Zeng X. Catalytic oxidative desulfurization of gasoline using phosphotungstic acid supported on MWW zeolite. Front Chem Sci Eng. 2020;14:546–60.
11. Yaseen M, Ullah S, Ahmad W, Subhan S, Subhan F. Fabrication of Zn and Mn loaded activated carbon derived from corn cobs for the adsorptive desulfurization of model and real fuel oils. Fuel. 2021;284:119102.
12. Jayne D, Zhang Y, Haji S, Erkey C. Dynamics of removal of organosulfur compounds from diesel by adsorption on carbon aerogels for fuel cell applications. Int J Hydrogen Energ. 2005;30:1287–93.
13. Fadhil AB, Saeed HN, Saeed LI. Polyethylene terephthalate waste-derived activated carbon for adsorptive desulfurization of dibenzothiophene from model gasoline: Kinetics and isotherms evaluation. Asia-Pac J Chem Eng. 2021;16:e2594.
14. Shah SS, Ahmad I, Ahmad W, Ishaq M, Gul K, Khan R, et al. Study on adsorptive capability of acid activated charcoal for desulphurization of model and commercial fuel oil samples. J Environ Chem Eng. 2018;6:4037–43.
15. Rezakazemi M, Zhang Z. Desulfurization materials. In: Dincer I, editor. Comprehensive Energy Systems. Oxford: Elsevier; 2018. p. 944–79.
16. Saha B, Vedachalam S, Dalai AK. Review on recent advances in adsorptive desulfurization. Fuel Process Technol. 2021;214:106685.
17. Sundararaman R, Ma X, Song C. Oxidative desulfurization of jet and diesel fuels using hydroperoxide generated in situ by catalytic air oxidation. Ind Eng Chem Res. 2010;49:5561–8.
18. Alcaraz MGT, Choi AES, Dugos NP, Wan MW. A review on the adsorptive performance of bentonite on sulfur compounds. Chem Engineer Trans. 2023;103:553–8.
19. Bhattacharyya KG, Gupta SS. Kaolinite, montmorillonite, and their modified derivatives as adsorbents for removal of Cu(II) from aqueous solution. Sep Purif Technol. 2006;50:388–97.
20. Choi AES, Roces S, Dugos N, Arcega A, Wan MW. Adsorptive removal of dibenzothiophene sulfone from fuel oil using clay material adsorbents. J Clean Prod. 2017;161:267–76.
21. Choi AES, Roces S, Dugos N, Wan MW. Adsorption of benzothiophene sulfone over clay mineral adsorbents in the frame of oxidative desulfurization. Fuel. 2017;205:153–60.
22. Ullah S, Hussain S, Ahmad W, Khan H, Khan KI, Khan SU, et al. Desulfurization of model oil through adsorption over activated charcoal and bentonite clay composites. Chem Eng Technol. 2020;43:564–73.
23. Yi D, Huang H, Li S. Desulfurization of model oil via adsorption by copper(II) modified bentonite. B Kor Chem Soc. 2013;34:777–82.
24. Ali FD. Adsorptive desulfurization of liquid fuels using na-bentonite adsorbents. Al-Nahrain J. Eng. Sci. 2018;21:248–52.
25. Ahmad W, Ahmad I, Ishaq M, Ihsan K. Adsorptive desulfurization of kerosene and diesel oil by Zn impregnated montmorollonite clay. Arab J Chem. 2017;10:S3263–S9.
26. Chen TC, Agripa ML, Lu MC, Dalida MLP. Adsorption of sulfur compounds from diesel with ion-impregnated activated carbons. Energy Fuel. 2016;30:3870–8.
27. Lu MC, Agripa ML, Wan MW, Dalida MLP. Removal of oxidized sulfur compounds using different types of activated carbon, aluminum oxide, and chitosan-coated bentonite. Desalin Water Treat. 2014;52:873–9.
28. Osibanjo R, Curtis R, Lai Z. Infrared Spectroscopy. Chemistry Library; 2023. https://chem.libretexts.org/@go/page/1847 (Accessed 23 Jul 2024).
29. Xiao H, Peng H, Deng S, Yang X, Zhang Y, Li Y. Preparation of activated carbon from edible fungi residue by microwave assisted K_2CO_3 activation—Application in reactive black 5 adsorption from aqueous solution. Bioresource Technol. 2012;111:127–33.
30. de Luna MDG, Flores ED, Genuino DAD, Futalan CM, Wan MW. Adsorption of Eriochrome Black T (EBT) dye using activated carbon prepared from waste rice hulls—Optimization, isotherm and kinetic studies. J Taiwan Inst Chem E. 2013;44:646–53.
31. Aguilar C, Garcia R, Soto-Garrido G, Arriagada R. Catalytic wet air oxidation of aqueous ammonia with activated carbon. Appl Catal B Environ. 2003;46:229–37.
32. Ishaq M, Sultan S, Ahmad I, Ullah H, Yaseen M, Amir A. Adsorptive desulfurization of model oil using untreated, acid activated and magnetite nanoparticle loaded bentonite as adsorbent. J Saudi Chem Soc. 2017;21:143–51.
33. Yi H, Nakabayashi K, Yoon SH, Miyawaki J. Pressurized physical activation: A simple production method for activated carbon with a highly developed pore structure. Carbon. 2021;183:735–42.
34. Pearson RG. Hard and Soft Acids and Bases. J Am Chem Soc. 1963;85:3533–9.
35. Revellame ED, Fortela DL, Sharp W, Hernandez R, Zappi ME. Adsorption kinetic modeling using pseudo-first order and pseudo-second order rate laws: A review. Clean Eng Technol. 2020;1:100032.

36. Toor M, Jin B. Adsorption characteristics, isotherm, kinetics, and diffusion of modified natural bentonite for removing diazo dye. Chem Eng J. 2012;187:79–88.
37. Chen TC, Sapitan JFF, Ballesteros FC, Lu MC. Using activated clay for adsorption of sulfone compounds in diesel. J Clean Prod. 2016;124:378–82.
38. Al-Ghouti MA, Da'ana DA. Guidelines for the use and interpretation of adsorption isotherm models: A review. J Hazard Mater. 2020;393:122383.
39. Tran HN, You SJ, Hosseini-Bandegharaei A, Chao HP. Mistakes and inconsistencies regarding adsorption of contaminants from aqueous solutions: A critical review. Water Res. 2017;120:88–116.
40. Dubinin MM. The potential theory of adsorption of gases and vapors for adsorbents with energetically nonuniform surfaces. Chem Rev. 1960;60:235–41.
41. Araujo CST, Almeida ILS, Rezende HC, Marcionilio SMLO, Leon JJL, de Matos TN. Elucidation of mechanism involved in adsorption of Pb(II) onto lobeira fruit (Solanum lycocarpum) using Langmuir, Freundlich and Temkin isotherms. Microchem J. 2018;137:348–54.
42. Shah SS, Ahmad I, Ahmad W. Adsorptive desulphurization study of liquid fuels using Tin (Sn) impregnated activated charcoal. J Hazard Mater. 2016;304:205–13.
43. Al-Anber MA. Ch. 27 Thermodynamics approach in the adsorption of heavy metals. In: Juan Carlos MP, editor. Thermodynamics - Interaction Studies - Solids, Liquids and Gases. Rijeka: IntechOpen; 2011;737–64. https://www.intechopen.com/chapters/21870.
44. Ebelegi AN, Ayawei N, Wankasi D. Interpretation of adsorption thermodynamics and kinetics. Open J Phys Chem 2020;10:166–82.

Publisher's Note